scattering electrons – mostly due to single or multiple elastic events – and of an important fraction of inelastic electrons suffering more than one energy loss. The probability of having n inelastic processes of mean free path Λ is governed by the Poisson distribution:

$$P_n(t) = \frac{1}{n!}\left(\frac{t}{\Lambda}\right)^{-n} \exp\left(-\frac{t}{\Lambda}\right). \qquad (4.3.4.6)$$

Multiple losses introduce additional peaks in the energy-loss spectrum; they are also responsible for an increased background that complicates the detection of single characteristic core-loss signals. Consequently, when the specimen thickness is not very small (*i.e.* for $t \gtrsim 50$ nm for 100 keV primary electrons), it is necessary to retrieve the single scattering profile that is truly representative of the electronic and chemical properties of the specimen.

Deconvolution techniques have therefore been developed to remove the effects of plural scattering from the low-loss spectrum (up to 100 eV) or from ionization edges but very few treatments deal with both angle and energy-loss distributions. Batson & Silcox (1983) have made a detailed study of the inelastic scattering properties of incident 75 keV electrons through a ~100 nm thick polycrystalline aluminium film, over the full range of transferred wavevectors ($0 \rightarrow 3$ Å^{-1}) and energy losses ($0 \rightarrow 100$ eV). Schattschneider (1983) has proposed a matrix approach that is sufficiently elaborate to handle angle-resolved energy-loss data. Simpler deconvolution schemes have been proposed and used for processing multiple losses without specific consideration of angular truncation effects. They are valid when the data have been recorded over sufficiently large angles of collection so that all appreciable inelastic scattering is included. They are generally based on Fourier transform techniques, except for the iterative approach of Daniels, Festenberg, Raether & Zeppenfeld (1970), which has been used for energy losses up to about 60 eV (Colliex, Gasgnier & Trebbia, 1976). The most accurate current methods are the Fourier-log method of Johnson & Spence (1974) and Spence (1979), and the Fourier-ratio method of Swyt & Leapman (1982), which only applies to the core-loss region. The first is far more complete and accurate and applies to any spectral range when one has recorded a full spectrum in unsaturated conditions.

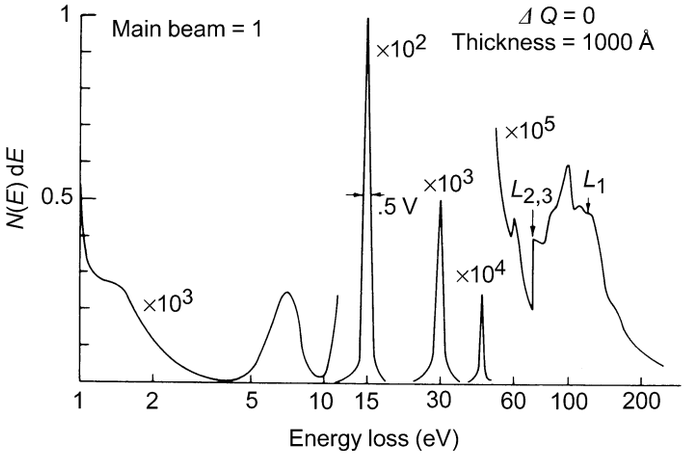

Fig. 4.3.4.3. Excitation spectrum of aluminium from 1 to 250 eV, investigated by EELS on 300 keV primary electrons [courtesy of Schnatterly (1979)].

4.3.4.1.4. *Classification of the different types of excitations contained in an electron energy-loss spectrum*

Figs. 4.3.4.3 and 4.3.4.4 display examples of electron energy-loss spectra over large energy domains, typically from 1 to about 2000 eV. With one instrument, all elementary excitations from the near infrared to the X-ray domain can be investigated. Apart from the main beam or zero-loss peak, two major families of electronic transitions can be distinguished in such spectra:

(*a*) The excitations in the low or moderate energy-loss region ($1 < \Delta E < 50$ eV) concern the quasifree (valence and conduction) electron gas. In a pure metal, such as Al, the dominant feature is the intense narrow peak at 15 eV with its multiple satellites at about 30, 45, and 60 eV. One also detects an interband transition at 1.5 eV and a surface plasmon peak at ~ 7 eV. For the more complex mineral specimen, rhodizite, this contribution lies in the intense and broad, but not very specific, peak around 25 eV. All these features are discussed in detail in Subsection 4.3.4.3.

(*b*) The excitations in the high-energy-loss domain ($50 < \Delta E < 2000$ eV) concern excitation and ionization processes from core atomic orbitals: in Al, the $L_{2,3}$ edge is associated with the creation of holes on the $2p$ level, L_1 is due to the excitation of $2s$, and K of $1s$ electrons. These contributions appear as edges superposed on a regularly decreasing background. In the complex specimen, the succession of these

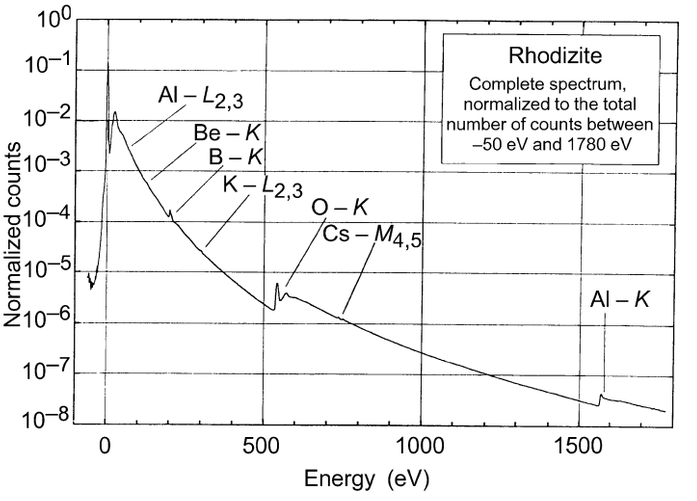

Fig. 4.3.4.4. Complete electron energy-loss spectrum of a thin rhodizite crystal (thickness ~60 nm). Separate spectra from eight significantly overlapping energy ranges were measured and matched. Primary energy 60 keV. Semi-angle of collection 5 mrad. Recording time 300 s (parallel acquisition). Scanned area 30×40 nm. Analysed mass 2×10^{-15} g [courtesy of Engel, Sauer, Zeitler, Brydson, Williams & Thomas (1988)].

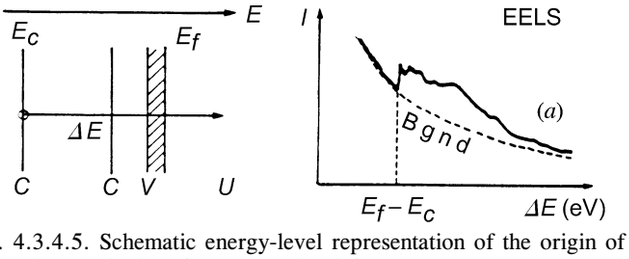

Fig. 4.3.4.5. Schematic energy-level representation of the origin of a core-loss excitation (from a core level C at energy E_c to an unoccupied state U above the Fermi level E_f) and its general shape in EELS, as superimposed on a continuously decreasing background.

different edges on top of the monotonously decaying background is a signature of the elemental composition, the intensity of the signals being roughly proportional to the relative concentration in the associated element. Core-level EELS spectroscopy therefore investigates transitions from one well defined atomic orbital to a vacant state above the Fermi level: it is a probe of the energy distribution of vacant states in a solid, see Fig. 4.3.4.5. As the excited electron is promoted on a given atomic site, the information involved has two specific characters: it provides the local atomic point of view and it reflects the existence of the hole created, which can be more or less screened by the surrounding population of electrons in the solid. The properties of this family of excitations are the subject of Subsection 4.3.4.4.

The non-characteristic background is due to the superposition of several contributions: the high-energy tail of valence-electron scattering, the tails of core losses with lower binding energy, *Bremsstrahlung* energy losses, plural scattering, *etc*. It is therefore rather difficult to model its behaviour, although some efforts have been made along this direction using Monte Carlo simulation of multiple scattering (Jouffrey, Sevely, Zanchi & Kihn, 1985).

When one monochromatizes the natural energy width of the primary beam to much smaller values (about a few meV) than its natural width, one has access to the infrared part of the electromagnetic spectrum. An example is provided in Fig. 4.3.4.6 for a specimen of germanium in the energy-loss range 0 up to 500 meV. In this case, one can investigate phonon modes, or the bonding states of impurities on surfaces. This field has been much less extensively studied than the higher-energy-loss range [for references see Ibach & Mills (1982)].

Generally, EELS techniques can be applied to a large variety of specimens. However, for the following review to remain of limited size, it is restricted to electron energy-loss spectroscopy on solids and surfaces in transmission and reflection. It omits some important aspects such as electron energy-loss spectroscopy in gases with its associated information on atomic and molecular states. In this domain, a bibliography of inner-shell excitation studies of atoms and molecules by electrons, photons or theory is available from Hitchcock (1982).

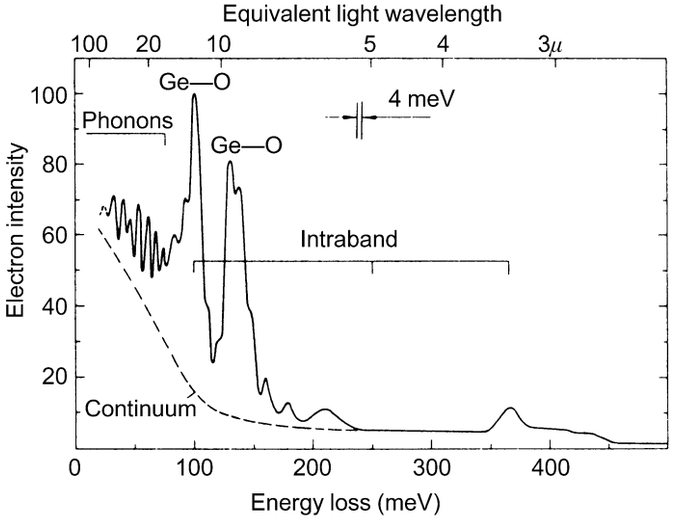

Fig. 4.3.4.6. Energy-loss spectrum, in the meV region, of an evaporated germanium film (thickness $\simeq 25$ nm). Primary electron energy 25 keV. Scattering angle $< 10^{-4}$. One detects the contributions of the phonon excitation, of the Ge—O bonding, and of intraband transitions [courtesy of Schröder & Geiger (1972)].

Table 4.3.4.1. *Different possibilities for using EELS information as a function of the different accessible parameters* (**r**, θ, ΔE)

	Integration parameter	Selection parameter	Results	Working mode of the spectrometer
1	**θ**	**r**	Spectrum $I_{\mathbf{r}}$ (ΔE)	Analyser
2	**r**	**θ**	Spectrum $I_{\boldsymbol{\theta}}$ (ΔE)	Analyser
3	**θ**	ΔE	Energy-filtered image $I_{\Delta E}(\mathbf{r})$	Filter
4	**r**	ΔE	Energy-filtered diffraction pattern $I_{\Delta E}(\boldsymbol{\theta})$	Filter

4.3.4.2. *Instrumentation*

4.3.4.2.1. *General instrumental considerations*

In a dedicated instrument for electron inelastic scattering studies, one aims at the best momentum and energy resolution with a well collimated and monochromatized primary beam. This is achieved at the cost of poor spatial localization of the incident electrons and one assumes the specimens to be homogeneous over the whole irradiated volume. In a sophisticated instrument such as that built by Fink & Kisker (1980), the energy resolution can be varied from 0.08 to 0.7 eV, and the momentum transfer resolution between 0.03 and 0.2 Å^{-1}, but typical values for the electron-beam diameter are about 0.2 to 1 mm. Nowadays, many energy-analysing devices are coupled with an electron microscope: consequently, an inelastic scattering study involves recording for a primary intensity I_0, the current $I(\mathbf{r}, \boldsymbol{\theta}, \Delta E)$ scattered or transmitted at the position **r** on the specimen, in the direction **θ** with respect to the primary beam, and with an energy loss ΔE. Spatial resolution is achieved either with a focused probe or by a selected area method, angular acceptance is defined by an aperture, and energy width is controlled by a detector function after the spectrometer. It is not possible from signal-to-noise considerations to reduce simultaneously all instrumental widths to very small values. One of the parameters (**r**, **θ** or ΔE) is chosen for signal integration, another for selection, and the last is the variable. Table 4.3.4.1. classifies these different possibilities for inelastic scattering studies.

Because of the great variety of possible EELS experiments, it is impossible to build an optimum spectrometer for all applications. For instance, the design of a spectrometer for low-energy incident electrons and surface studies is different from that for high-energy incident electrons and transmission work. In the latter category, instruments built for dedicated EELS studies (Killat, 1974; Gibbons, Ritsko & Schnatterly, 1975; Fink & Kisker, 1980; *etc*.) are different from those inserted within an electron-microscope environment, in which case it is possible to investigate the excitation spectrum from a specimen area well characterized in image and diffraction [see the reviews by Colliex (1984) and Egerton (1986)].

The literature on dispersive electron–optical systems (equivalent to optical prisms) is very large. For example, the theory of uniform field magnets, which constitute an important family of analysing devices, has been extensively developed for the components in high-energy particle accelerators (Enge, 1967; Livingood, 1969). As for EELS spectrometers, they can be classified as: